Chemical Science

ROYAL SOCIETY OF CHEMISTRY

PERSPECTIVE

View Article Online
View Journal | View Issue



Cite this: *Chem. Sci.*, 2023, **14**, 8984

All publication charges for this article have been paid for by the Royal Society of Chemistry

# Impact of core–shell perovskite nanocrystals for LED applications: successes, challenges, and prospects

Samrat Das Adhikari, [a] Andrés F. Gualdrón Reyes, [b] Subir Paul,[a] Jeevan Torres,[a] Beatriu Escuder, [a] Iván Mora-Seró [a] and Sofia Masi *[a]

Perovskite nanocrystals (PeNCs) synthesized by colloidal solution methods are an outstanding case of study due to their remarkable optical features, different from their bulk counterpart, such as a tuneable band gap and narrower photoluminescence emission, altered by the size and shape. However, the stability of these systems needs to be improved to consolidate their application in optoelectronic devices. Improved PeNC quality is associated with a less defective structure, as it affects negatively the photoluminescence quantum yield (PLQY), due to the essential, but at the same time labile interaction between the colloidal capping ligands and the perovskite core. In this sense, it would be extremely effective to obtain an alternative method to stabilize the PeNC phases and passivate the surface, in order to improve both stability and optical properties. This objective can be reached exploiting the structural benefits of the interaction between the perovskite and other organic or inorganic materials with a compatible structure and optical properties and limiting the optical drawbacks. This perspective contemplates different combinations of core/shell PeNCs and the critical steps during the synthesis, including drawbacks and challenges based on their optical properties. Additionally, it provides insights for future light emitting diode (LED) applications and advanced characterization. Finally, the existing challenges and opportunities for core/shell PeNCs are discussed.

Received 9th June 2023
Accepted 13th July 2023

DOI: 10.1039/d3sc02955g

rsc.li/chemical-science



## 1. Introduction

Halide perovskite nanocrystals (PeNCs) have gained significant attention in recent years due to their unique optical properties, including high colour purity and tuneable visible emission.[1–4] These properties make them ideal candidates for use in light-emitting diodes (LEDs), which require high PLQY and efficient light emission to function effectively. Lead halide perovskites are direct bandgap semiconductors and emit visible light through free excitons (FEs). In contrast, most lead-free perovskites (LFPs) exhibit photoemission primarily through self-trapped excitons (STEs), with a minority emitting through FEs. Similarly Pb-free double perovskites are more likely to emit through STEs due to their higher disorder and defect density.[5] However, there are some 0D lead-free perovskites, such as $A_3M_2X_9$ (A = $Cs^+$, methylammonium; M = $Bi^{3+}$, $Sb^{3+}$) that exhibit FE emission, which could make them useful for optoelectronic applications.[6,7] In recent years, researchers have been exploring the use of PeNCs in LEDs.[8–11] One of the key challenges in this area is achieving high external quantum efficiency (EQE), which is a measure of how efficiently the optoelectronic device converts electrical energy into light. One approach for improving the EQE of halide perovskite LEDs has been the use of PeNCs as an active layer instead of bulk thin films. This is because the smaller size of the nanocrystals offers better carrier confinement and crystalline quality in addition to surface passivation, which can reduce non-radiative recombination and improve the overall efficiency of the device. However, the limited stability in PeNCs somehow limits the widespread of perovskite nanocrystal based technological developments. The major concerns regarding the stability of PeNCs are surface trap states, environmental changes, photo-oxidative degradation, *etc.*[12,13] In some way, the same problems are also faced by metal chalcogenide quantum dots and nanocrystals.[14] In such cases, shelling with another nanocrystalline materials addressed these problems and dramatically enhanced their optical performances, ambient stability, and protection of the core materials.

Core/shell nanostructures for chalcogenide quantum dots have been studied over decades for the development of lighting device technologies.[15] In the case of perovskite-based core/shell nanocrystals,[16–18] the research is on the edge-on-the-seat for the development of perovskite LED (PeLED) performances. A detailed description of the types of core/shell structures is given in a later section, establishing how the core/shell structure is beneficial for favouring PeLED performance. In some of the

[a]*Institute of Advanced Materials (INAM), Universitat Jaume I (UJI), Avenida de Vicent Sos Baynat, s/n, Castelló, 12071, Spain*

[b]*Facultad de Ciencias, Instituto de Ciencias Químicas, Isla Teja Universidad Austral de Chile Valdivia, 5090000, Chile*

recent reports, the following points are addressed, which can deal with the challenges of PeLED implementation:[17]

(i) optical enhancement: recovery of surface defects, with protective shelling over perovskite nanocrystals, leads to reduction of non-radiative recombination and hence increasing radiative carrier recombination (*i.e.*, free excitons), increasing the photoluminescence quantum yield (PLQY).[19] Higher PLQY offers more efficient conversion of electrical energy into light energy, which results in brighter and more efficient LEDs.[20–22] Besides, the core–shell type-II heterostructure formation improves PL lifetime, stability, and LED performance.[19,23–25] It is noteworthy that some of the reports on 3D/0D core/shell perovskites observed shortening of lifetime in comparison to primitive (core-only), where the 0D materials have a wide bandgap and hence the core/shell materials show type-I heterostructure formation, ensuring a faster exciton decay.[21,26]

(ii) Tuneable emission: the optical emission can be easily tuned by A-site variable perovskite shelling over the perovskite core due to the alloy formation with smaller/larger A-site cations, which eventually reduces the average particle size and in turn offers blue-shifting.[27] This tuneability can be achieved by controlling the composition of the core and shell materials. This property allows the development of LED devices with different colours.

(iii) Stability improvement: halide perovskites experience temperature, light and moisture exposed degradation, which have been prevented by a coating with inorganic/organic materials on the core perovskite. One of the main issues in the fabrication of efficient optoelectronic technologies based on perovskite nanocrystals (PeNCs) such as LEDs is the relatively low stability of the phosphor material.[28] Due to their ionic nature, the facile loss of cationic/anionic species from the perovskite structure stimulates elemental vacancy related defect states.[29] In consequence, a high density of defect sites is formed, decreasing the optical performance of the active layer integrated into the device.[2,30,31] In this sense, several shelling strategies are employed to restrain the influence of moisture, high temperatures and harsh polar environments on the PeNC structural integrity, without hindering the carrier transport into the LED devices, discussed vividly in a later section.

## 2. Types of core/shell perovskite nanocrystals

PeNC based core/shell nanostructures are semiconductor heterostructures, where their physical properties relied on the corresponding band alignment, classified as type-I and type-II heterojunctions.[32] In the case of type-I heterojunctions, the valence band (VB) and conduction band (CB) of a smaller bandgap material are coincident of a larger bandgap material, and therefore the generated electrons and holes are confined within the same region. In the case of type-II heterojunctions, there is a "Z" type band alignment between the VB and CB of the core and shell materials (see Scheme 1).

Conceptually, type-I semiconductors are favourable for LED and lasing applications, due to the exciton confinement, whereas type-II semiconductors are extensively used for catalysis and energy cascade applications, due to the charge separation. However, in a recent report by Ye *et al.*, efficient LED device performance has been achieved from type-II perovskite/semiconductor core/shell nanostructures.[25] Shelling of the nanostructured crystals can be classified as single core/shell type and multiple core/shell type. In a single core/shell, there is a single shelling material, which can be an inorganic semiconductor,[19,23,24] a multidimensional perovskite core/shell alloy,[21] or organic polymer coated PeNCs.[33–35] In the case of multiple core/shell nanoparticles, they are formed when many smaller sized nanocrystals are coated with a single shelling material. This type of shelling has been studied extensively in the case of cubic-shaped perovskite nanocrystals, where several arrangements of nanocubes can be easily encapsulated by organic or inorganic protective materials.[36]

Considering all the possible perovskite nanocrystal-based core/shell materials, a classification is presented in Scheme 2, and their particulars are elaborated in the following sections.

### 2.1 Semiconductor/organic passivator core/shell

The organic coating around colloidal perovskite nanocrystals can be composed of both polymers and small molecules. Organic shelling of nanoparticles provides the opportunity of

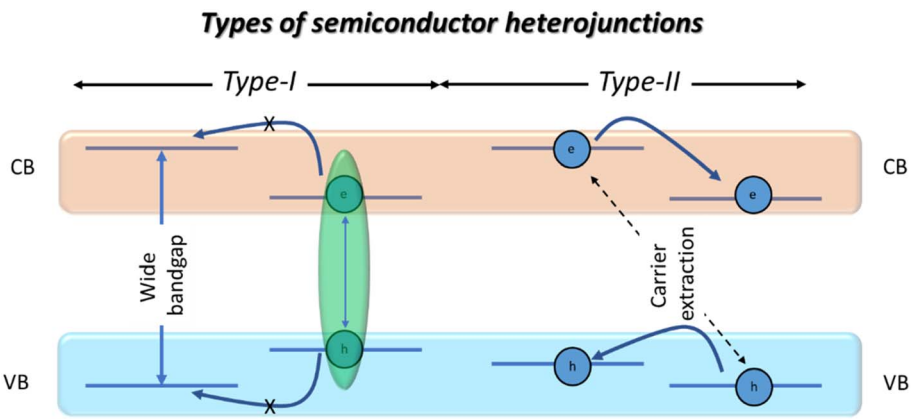


Scheme 1 A schematic representation of type-I and type-II heterojunctions in typical core/shell nanostructures.

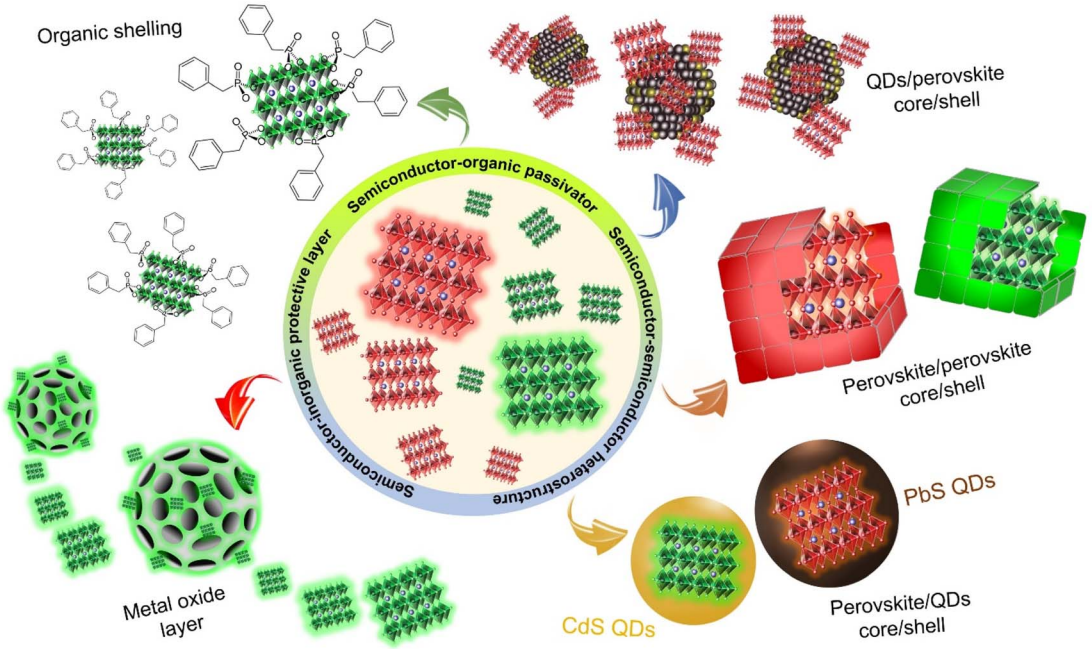


Scheme 2 Classification of core/shell perovskite nanocrystals.

tapping into beneficial traits such as reduced toxicity and increased stability against common threats such as heat and moisture.[37] In terms of stability, organic shelling can sometimes be proved as a double-edged sword in the case of perovskite nanoclusters as shown by Urban and coworkers.[38] They fabricated methylammonium lead bromide ($MAPbBr_3$) nanoclusters encapsulated inside core–shell micelles of a diblock copolymer comprising a combination of polystyrene (PS) and poly(2-vinylpyridine)(P2VP). The core–shell micelles were formed in toluene where the P2VP block forms the core and PS acts as the shell. The subsequent addition of the perovskite precursors in two steps resulted in the crystallization of halide perovskite within the micelles. Energy transfer *via* Fluorescence Resonance Energy Transfer (FRET) was measured between micelle encapsulated $MAPbBr_3$ nanoclusters and $CsPbBr_3$ nanoplatelets. It was observed that the best energy transfer efficiency was encountered in the case of the lowest shell thickness of micelles while the highest stability of drop-casted thin films under ambient conditions was encountered in the case of the thickest micelles. The authors, therefore, advocated the importance of finding a sweet spot between protection and activity for optimum device applications with these kinds of core–shell materials. In this regard, Fei and coworkers reported an interesting case where the shelling polymer material poly(norepinephrine) (PNE) is itself a photoactive material capable of light harvesting.[39] They constructed a core–shell system with methylammonium lead bromide ($MAPbr_3$, M-PE) nanoparticles encapsulated inside (PNE) thin layers, and the schematic is presented in Fig. 1a. A core–shell system with a 10 nm thick shell of PNE, see Fig. 1b, not only exhibited higher stability against moisture exposure but also showed eight times higher photocatalytic efficiency towards the degradation of malachite green dye compared to that of pristine M-PE. However, a further increase in the thickness of the shell leads to a decreased photocatalytic efficiency, which again points towards the necessity of accomplishing an optimum thickness of the organic shell (even if it is photoactive) for the best performance. Hence, based on these reports, the optimal organic shell thickness for the perovskite core is a trade-off between stability and charge transport capabilities, crucial for achieving superior optoelectronic device performance.

Lee and coworkers recently came up with a breakthrough finding regarding the shelling of perovskite nanocrystals with organic molecules for PeLED applications.[40] They found out that post-treatment of a 3D perovskite film of $(FA_{0.7}MA_{0.1}GA_{0.2})_{0.87}Cs_{0.13}PbBr_3$ with benzylphosphonic acid (BPA) results in BPA capped core–shell nanocrystals, which show a very strong PLQE of 85%. This report indicates that discrete single core/shell nanostructures are formed as BPA molecules penetrate the large grain of perovskite thin films. A schematic of such a mechanism is presented in Fig. 1c. The TEM image of BPA-shelling over perovskite nanocrystals is presented in Fig. 1d. Based on this observation, it has been concluded that the shelling of BPA ligands results in the binding of non-bonded Pb atoms, thereby reducing trap density, minimizing carrier extraction, and increasing carrier confinement, ultimately leading to enhanced luminous efficiency. These beneficial gains accompanying the transformation into a core–shell nanocluster are manifested by the unprecedented LED performance exhibited by the system. LEDs fabricated with the core–shell nanocluster system exhibited a maximum current efficiency of 151 cd $A^{-1}$ and a maximum EQE of 28.9% with a maximum brightness of 473 990 cd $m^{-2}$, which is comparable

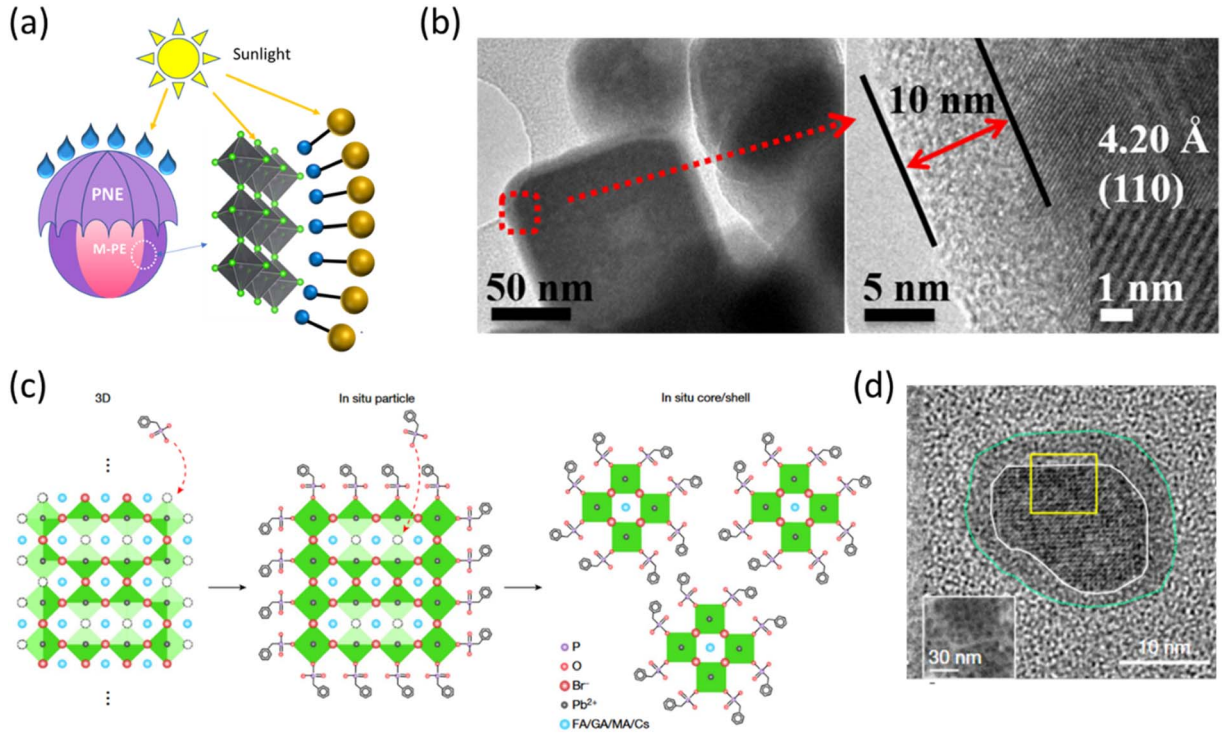


Fig. 1 (a) A schematic of $MAPbBr_3$ (M-PE) perovskite core/poly(norepinephrine) (PNE) shell nanocrystals, and (b) the corresponding TEM images of wide and enlarged views showing a 10 nm thick shell of PNE micelles over perovskite. Reproduced with permission from ref. 39, Copyright © 2020, American Chemical Society. (c) Schematic of the BPA-induced core–shell formation mechanism. (d) TEM image of a $(FA_{0.7}MA_{0.1}GA_{0.2})_{0.87}Cs_{0.13}PbBr_3$ core/BPA shell nanocrystal. Reproduced with permission from ref. 40 Spring Nature.

with the highest brightness of state-of-the-art inorganic quantum dot LEDs, and the record performance for PeLEDs.[41]

Proper organic capping also allows an increase of performance for photocatalytic applications. As an example, the stability improvement has been demonstrated in alcoholic media through the introduction of organic coordinated ligands.[42] However, the instability in water is a significant concern that needs to be addressed to utilize perovskite nanocrystals in various applications. Very recently, Rao and co-workers have reported a short-chain multidentate bolaamphiphilic ligand (NKE-3), able to passivate the perovskite surface with an ionic terminal bearing amino functionalities and interact with water molecules with a terminal glutamic acid, leading to a water suspended colloidal solution of PeNCs.[43] This system allowed an efficient long-range dipole-based FRET from perovskites to Rhodamine B isothiocyanate (RITC) in water, with FRET efficiencies ranging from 96% to 98%. Additional research is required to enhance the operational durability of PeLEDs that are coated with an organic material under moist conditions to make them suitable for practical applications.

The use of core–shell nanoparticles with organic/polymer shelling for optoelectronic devices has to provide enough electrical integration as the coating is non-conductive in most cases. Thus, the major synthetic challenge would be to reap the benefits of organic shelling, such as enhanced stability, without compromising the optoelectronic properties of perovskites. One way to achieve this goal is obviously tuning the thickness of the organic shell to an optimum value. In addition, the characteristics of each ligand also will influence the selection of organic molecules for shelling. Molecules that can directly interact with the metal could be better candidates as shell materials compared to those which only form a non-interacting shell as evidenced by the findings of Lee and co-workers.[40]

### 2.2 Semiconductor/semiconductor heterostructure

This class of core/shell structures can be classified into three subcategories based on the arrangement of the perovskite material as the core or shell component of the structure. In the first subcategory, the core is made of perovskite while a non-perovskite semiconductor (typically, metal chalcogenides) forms the shell. In the second subcategory, the shell is made of perovskite while the core is composed of another perovskite material by altering the dimensions of the perovskite or changing the A-site cation of the perovskite. Finally, the third subcategory involves perovskite being utilized exclusively as the shell material.

**2.2.1 Perovskite/semiconductor core/shell.** The common effects and motivations of using the core/shell structure in perovskite and non-perovskite semiconductor materials (such as metal chalcogenides) are evident, as they both aim to provide moisture protection to the material and passivation by suppressing surface vacant states.[36,44–46] Nonetheless, a critical factor also pertains to the core/shell arrangement that enables the creation of heterostructures, thereby facilitating appropriate

band alignment to support optoelectronic and catalytic functions.[32,47,48] Regarding LED device applications, some reports have been published on their pioneering activities such as stability and enhanced optical activities, and a benchmark has been established to advance their future LED applications.[26,49–51]

The epitaxial growth of the shell material, which faces strain related to lattice mismatch, is evidently the primary challenge in designing any core/shell material. In this context, the lattice constant of $CsPbBr_3$ is 5.85 Å and CdS is 5.83 Å,[24,52] which closely match the values of lattice constants. This fact enables the formation of a less strained interface in the $CsPbBr_3$/CdS nanostructure.[19,53–55] The synthesis and optical properties of a $CsPbBr_3$/CdS core/shell heterostructure were investigated by Kipkorir *et al.*[24] The study revealed that CdS capping effectively suppresses defect states at the surface of core $CsPbBr_3$ nanocrystals. This core/shell nanocrystals exhibit a nearly seven-fold increase in time-resolved PL lifetime compared to pristine $CsPbBr_3$ nanocrystals, see Fig. 2a, which is an additional advantage of the core/shell structure in addition to surface passivation. The heterostructure formation facilitates the formation of quasi type-II band alignment, see Fig. 2b, where the nearly isoenergetic conduction band of core $CsPbBr_3$ and shell CdS offers delocalization of electrons across two semiconductors, prompting charge separation.

Another exciting performance of ZnS nanolayer coating over $CsPbBr_3$ nanocubes has been reported by Ravi *et al.*,[23] which also established nearly 15 times extended PL lifetime of the $CsPbBr_3$/ZnS core/shell nanostructure in comparison to core-only $CsPbBr_3$ nanocrystals, see Fig. 2c. As explained in the previous paragraph, heterostructure formation due to the coating of a metal chalcogenide layer over the perovskite electronically facilitates the PL lifetime. In this example, the valence band maximum is in a similar position to that of $CsPbBr_3$, and the conduction band minimum is significantly higher than that of $CsPbBr_3$, and then they form a quasi-type-II heterostructure, where the hole is delocalised with the core and shell and the electron is localised in the core material, see Fig. 2d. From this observation, the significant PL lifetime enhancement is explained. The high-resolution TEM image of the epitaxial heterojunction of $CsPbBr_3$ and ZnS is presented in Fig. 2e. In this work, the authors have also studied the water and photostability of the nanostructure.

From these recently developed reports on perovskite/chalcogenide core/shell nanostructures, PL lifetime enhancement is the common effect that has been established. In this context, a longer lifetime can result in a more stable and consistent emission of light over time, which is important for practical applications of LEDs, where uniform and long-lasting lighting is needed, which could be a potential aspect of $CsPbBr_3$/MS (M = Zn, Cd) core/shell nanocrystals for future implementation as a PeLED.

Lead chalcogenide is found to be an efficient chalcogenide-based shelling semiconductor because of common metal ions ($Pb^{2+}$, herein). In a report by Zhang *et al.*, PbS shelling $CsPbI_3$ nanocrystals are constructed for the application of efficient and stable PeLEDs. The PbS-shelling not only passivated the $CsPbI_3$, but also induced a switch in its semiconducting behaviour from n-type to ambipolar. As a result, the PeLED's

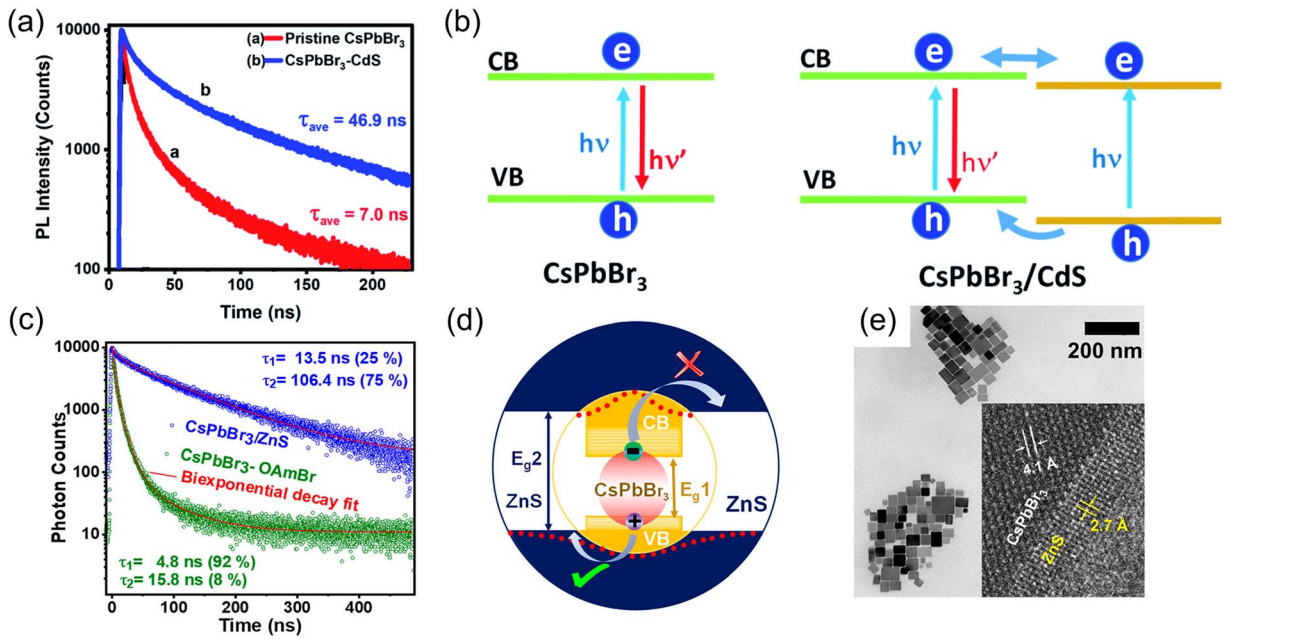


Fig. 2 (a) Time-resolved PL lifetime of the $CsPbBr_3$/CdS core/shell nanostructure showing enhanced lifetime comparison to the pristine. (b) Schematic of the presentation of carrier recombination of the carrier transfer process of pristine $CsPbBr_3$ and $CsPbBr_3$/CdS core/shell nanostructures. Reproduced from ref. 24 under the terms of the CC-BY license. (c) PL lifetime of $CsPbBr_3$/ZnS showing 15 times enhancement in comparison to the control ($CsPbBr_3$-oleylammonium bromide capped). (d) Schematic of the $CsPbBr_3$/ZnS core/shell band structure showing typical charge separation in the semiconductor heterojunction. (e) HR-TEM image of the typical heterojunction of the $CsPbBr_3$–ZnS core/shell heterojunction. Reproduced from ref. 23 with permission, Copyright © 2020, American Chemical Society.

electroluminescence occurred in a p–i–n structure.[46] Furthermore, the effectiveness of PbS-shelling is demonstrated by its tolerance to polar solvents in a case study involving $CsPbBr_3$/PbS core/shell nanostructures.[45]

The perovskite/chalcogenide semiconductors have been synthesized successfully; however, there are some limitations in the synthesis of a wide range of metal chalcogenide shelling following the colloidal synthesis strategy. The challenge in this synthesis lies in the following factors: (i) separate growth of the chalcogenide nanocrystals, (ii) degradation of perovskite nanocrystals in the presence of the shelling precursor materials, and (iii) reaction temperature that leads to uncontrolled growth of shelling materials, and at the same time perovskite nanocrystal ripening/agglomeration. To overcome these synthesis obstacles, Ravi *et al.* synthesized $CsPbBr_3$/ZnS core/shell nanocrystals using $Zn(DDTC)_2$ as a single molecular precursor to grow a ZnS shell epitaxially over the $CsPbBr_3$ core, where the shelling procedure do not interfere to degrade the core perovskite. The single molecular precursor slowly releases Zn and S at lower temperature, and hence the chances of separate growth of ZnS quantum dots are ruled out. $CsPbBr_3$/ZnS nanocrystals are synthesized by the low temperature ZnS shell growth and the slow release of the precursor, which eventually prevents the separate nucleation of the ZnS impurity phase.[23]

**2.2.2 Perovskite/perovskite core/shell.** Perovskite/perovskite core/shell heterostructures can be subcategorized into three main types based on the dimensions of the constituent components:

(i) 3D/3D core/shell heterostructures consist of a 3D perovskite core and a 3D perovskite shell, where the two perovskites have different compositions or crystal structures. In the case of 3D/3D core/shell heterostructures, shelling of 3D perovskites over 3D perovskite nanocubes has been reported to provide better photophysical performances. In this way, Yang and coworkers[50] have developed the colloidal synthesis of core/shell PeNCs, through the epitaxial growth of $CsPbBr_3$ on $FAPbBr_3$ PeNCs, see the schematic presented in Fig. 3c. The core-only $FAPbBr_3$ nanocrystals exhibit an average particle size of $8.2 \pm 1.2$ nm. Upon shelling with $CsPbBr_3$ at an FA : Cs molar ratio of 1, the average particle size increases to $11.2 \pm 1.1$ nm, see Fig. 3d. The resultant $FAPbBr_3$@$CsPbBr_3$ nanocrystal composite solutions exhibit a PLQY of up to 93% and are stable under ambient conditions for 70 days and resistant to continuous UV illumination for 50 h. The combination of both kinds of nanoparticles induces the emergence of alloyed $FA_xCs_{1-x}PbBr_3$ at the core/shell interface, favoring the surface defect passivation and thereby the improvement of radiative carrier recombination. This modification can be observed through the electroluminescence (EL) spectra of the materials, achieving a displacement of the EL peak position of the PeNCs by varying the thickness of the $CsPbBr_3$ shell. In this way, green-LEDs were fabricated with a maximum EQE of ~8.1%, luminance ($L$) of ~1758 cd $m^{-2}$, initial operation voltage ($V_{ON}$) = 2.6 V and a maximum operational lifetime ($T_{50}$) of ~ 47 min, at $L = 100$ cd $m^{-2}$.

(ii) 3D/2D core/shell heterostructures consist of a three-dimensional (3D) perovskite core and a two-dimensional (2D) perovskite shell. In the case of 3D/2D, 2D perovskites are composed of hybrid organic-inorganic materials and their heterojunctions are formed through van der Waals epitaxy. In the case of van der Waals heterostructures,[56] the capping ligands (act as a spacer cation) attached to the halides can have possible interaction with a next inorganic layer(s) surrounding the 3D perovskite nanocubes. Eventually, this type of interaction leads to the development of a 3D perovskite structure featuring a layer of 2D perovskite.[57,58] In principle, the category of such a kind of shelling is a single core/shell type, where the individual nanocubes are shelled by 2D perovskite layers. As an example, a single layer of guanidinium lead halide over 3D perovskites acts as the 2D perovskite shell over 3D perovskite nanocrystals, which has been studied in a few recent reports. This configuration passivates the surface trap states and improves the carrier transportation for the solar cell performance. The benefits of guanidium cations are attributed to their strong hydrogen bonding ability with the surface halides, which in turn facilitates the surface defect recovery.[58–61] 3D/2D core/shell perovskites are regarded as multidimensional perovskites, where Chen *et al.* revealed that the multidimensional type-I heterostructure formation between 3D $MAPbBr_3$ and 2D $(octylammonium)_2PbBr_4$ leads to multiphoton absorption, which are useful for multiphoton imaging applications.[62] In a recent report by Ye *et al.*,[25] spin-polarised luminescence behaviour has been studied, where a chiral organic ammonium bromide molecule is introduced to provide a 2D perovskite layer coating, which formed a 3D/2D core/shell with a type-II heterostructure. In this study, the chiral shell acts as a spin-filter to select the spin to inject into the achiral core, which eventually imparts the spin polarised properties to the achiral $MAPbBr_3$ core. This effect is finally applied to the room temperature spin-LED application to obtain spin polarised electroluminescence. Fig. 3a provides the schematic of such an achiral $MAPbBr_3$ core/chiral 2D organic ammonium bromide shell (upper panel), and the TEM image (lower panel) of $MAPbBr_3$/(S/R)-(+/−)-α-methylbenzenemethanammonium lead bromide ($^{S/R}PEA_2PbBr_4$) core/shell. A thin layer of $^{S/R}PEA_2PbBr_4$ 2D perovskite surrounding the achiral $MAPbBr_3$ core is clearly observed from the TEM image (Fig. 3b), where the thin layer controls the spin-selective injection into the core $MAPbBr_3$.

(iii) 3D/0D core/shell heterostructures consist of a 3D perovskite core and zero-dimensional (0D) perovskite nanoparticles on the surface. 3D/0D core/shell perovskites refer to the epitaxial shelling of a 0D perovskite onto a 3D perovskite. Although $FAPbBr_3$ (with a bandgap of 2.18 eV) has been found to be a superior ultrapure green emitter compared to $CsPbBr_3$ (with a bandgap of 2.25 eV), the hybrid organic-inorganic $FAPbBr_3$ is much less stable than the all-inorganic $CsPbBr_3$. However, by shelling the $FAPbBr_3$ core with 0D $Cs_4PbBr_6$ perovskite, a recent study by Zeng *et al.*[21] has demonstrated high stability with improved emission. The presented heterojunction is of the type-I category, wherein the core material has a bandgap of approximately 2.18 eV and the shell material has a bandgap of around 4.0 eV. Fig. 3f depicts the atomic model of the $FAPbBr_3$ core and the sequential growth of $Cs_4PbBr_6$ through the creation of a mixed alloy transition layer of $FA_xCs_{1-x}PbBr_3$. The shelling process involves the

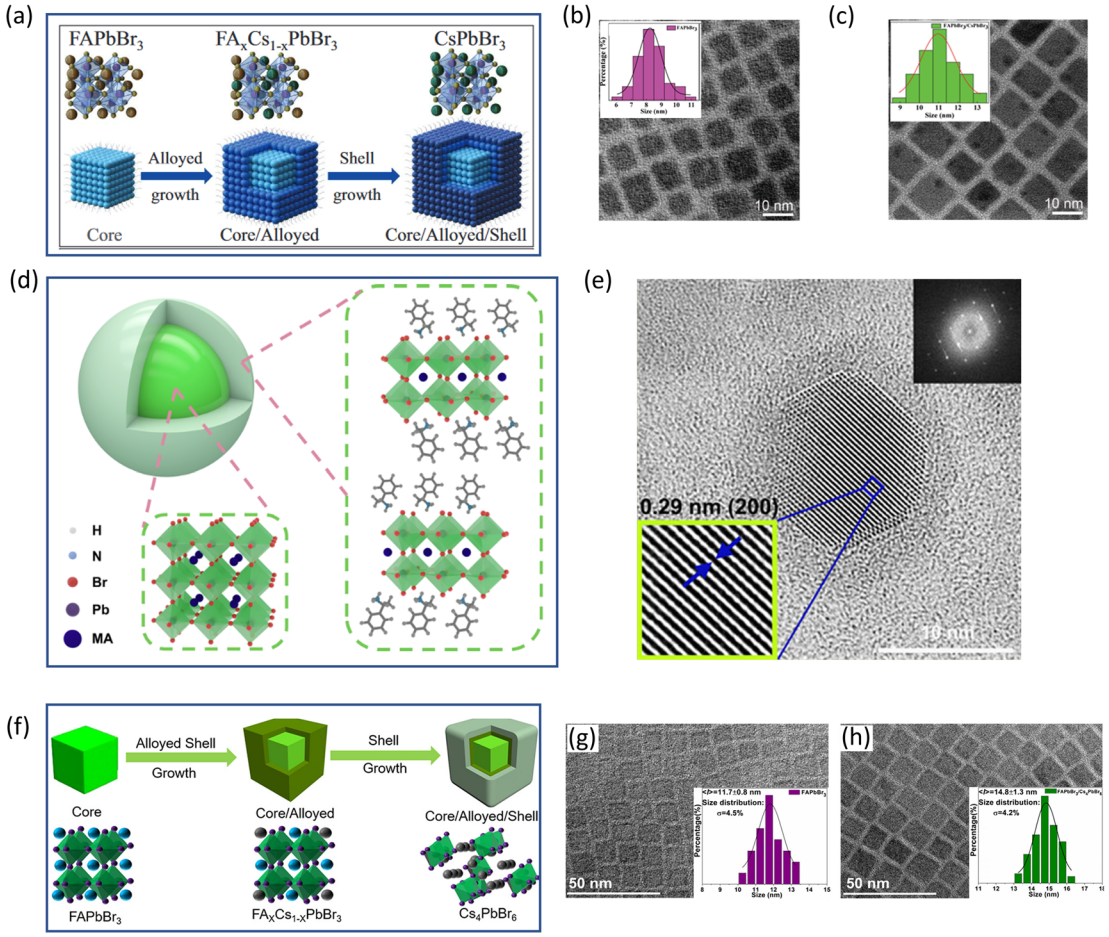


Fig. 3 3D/3D core/shell: (a) schematic presentation of the epitaxial growth of $CsPbBr_3$ on $FAPbBr_3$ PeNCs, and their TEM images and particle size histogram of (b) core-only $CsPbBr_3$ and (c) core/shell $CsPbBr_3/FAPbBr_3$ PeNCs. Reproduced with permission from ref. 50, under the terms and conditions from creative commons CC-BY license. 3D/2D core/shell: (d) schematic of the 2D/3D core/shell atomic model and (e) corresponding TEM image of a $MAPbBr_3/(^{S/R}PEA_2PbBr_4)$ core/shell nanocrystal. Reproduced from ref. 25 with permission, Copyright © 2020, American Chemical Society. 3D/0D core/shell: (f) schematic of the atomic model of the $FAPbBr_3$ core and the sequential growth of $Cs_4PbBr_6$ through the creation of a mixed alloy transition layer of $FA_xCs_{1-x}PbBr_3$, and their TEM images and particle size histogram of (g) core-only $FAPbBr_3$ and (h) core/shell $FAPbBr_3/Cs_4PbBr_6$ PeNCs. Reproduced from ref. 21 with permission, Copyright © 2020, American Chemical Society.

epitaxial growth of $Cs_4PbBr_6$ over $FAPbBr_3$ nanocubes, with $Cs^+$ ions partially penetrating the $FAPbBr_3$ lattice and reducing the lattice mismatch. The shelling is carried out seamlessly through the $FA_{1-x}Cs_xPbBr_3$ transition layer. The TEM images of $FAPbBr_3$ core-only and $FAPbBr_3/Cs_4PbBr_6$ core/shell nanocrystals are provided in Fig. 3g and h. Xu *et al.*[51] reported multiple core/shell perovskite nanocrystals embedded in another perovskite matrix useful for LED applications. They have prepared a green-emitting LED based on a $CsPbBr_3/Cs_4PbBr_6$ nanostructure using a solution growth thin film deposition technique.

Despite the success in the synthesis of core/shell perovskite nanocrystals, limitations can be encountered during the synthesis, where the first and foremost is the mixed phase formation instead of the core/shell. Despite the benefits of shelling upon the van der Waals interaction for 2D perovskites, their morphology is typically large sheets and it is hard to control the length of the sheets, which might be challenging for shelling over a 3D cubic shaped perovskite material, since it is very hard to grow a crystal over the cubic-shaped nanocrystals. The nanocubes have six planes and twelve edges, which makes it quite challenging to shell them with a different material, due to the limited formation potential caused by the restricted degree of freedom. In this context, Xu *et al.* designed the morphology of the $MAPbBr_3$ core material as spherical in $MAPbBr_3/^{S/R}PEA_2PbBr_4$ core/shell perovskite. It is anticipated that the shelling of the 2D material has less formation potential. In some reports, the challenges are overcome to have shelling over nanocubes, and among those reports, the synthesis of perovskite/perovskite $Cs_{1-x}FA_xPbBr_yI_{3-y}$ core/shell nanocrystals is carried out following a modified hot-injection method, where FABr in isopropyl alcohol and the protective alkylammonium iodide ligand in isopropyl alcohol was injected sequentially into colloidally dissolved lead iodide solution in the presence of oleic acid and oleylamine at 140 °C and 150 °C, respectively. In the following step, Cs-oleate was injected at 200 °C, and the reaction was quenched by rapid cooling in an ice bath. In this example, isopropyl alcohol helps to dissolve organic cations and

acts as an antisolvent to crystallize hybrid core/shell perovskite nanocrystals.[57]

In this regard, the synthesis challenges of core/shell perovskite/perovskite nanocrystals irrespective of the dimensions of the perovskites have been solved partially; however, some fundamental concepts are still in the embryo stage to elaborate. Table 1 depicts the synthesis challenges and their possible outcome:

### 2.3 Perovskite/inorganic protective layer core/shell

Prominent inorganic non-perovskite materials are designed for the coverage of PeNCs based on metal oxides,[63–65] sulfates,[66,67] phosphates,[68] tungstate,[69] and alkali metal halides,[70] or the synthesis of core–shell based PeNCs[17] to promote the passivation of surface defects and improve the radiative recombination mechanism. Brovelli and coworkers[71] have revealed the "resurfacing" concept to prepare $CsPbBr_3$ PeNCs for ultrabright LEDs. The authors performed the triple ligand method in which some quaternary ammonium salts such as didodecyldimethylammonium bromide (DDAB) are added during the hot-injection synthesis, and then they led to the *in situ* growth of a $NiO_x$ layer covering the nanocrystals. Accordingly, PeNCs with PLQY up to 100% are produced with enhanced electronic properties. This is caused by the partial removal of oleic acid and oleylamine ligands during $NiO_x$ treatment leaving DDAB moieties. In this context, the relative band structure of the different hole- and electron-transport layers composing the device is aligned with the PeNCs:$NiO_x$ composites, favoring an effective carrier injection and mobility into the active layer. The core/shell structure serves as a barrier to prevent moisture from reaching the active layer of the device, thus enhancing its long-term stability. This is particularly important for organic electronic devices as they are more susceptible to moisture-induced degradation than their inorganic counterparts. Furthermore, the formation of a $NiO_x$ heterostructure on the surface of the PeNCs enhances the carrier transport properties of the device. This is due to the synergistic band-alignment between the PeNCs and $NiO_x$, which improves the energy level alignment and facilitates efficient charge transfer. Overall, this study highlights the importance of core/shell structures in enhancing the stability of organic electronic devices and the potential of heterostructure formation for improving their performance. In this way, highly efficient green-LEDs were obtained with EL spectra with a peak centered at 514 nm, CIE color coordinates of (0.05, 0.66) ascribed to ~90% saturated green light, see Fig. 4a, a maximum EQE of ~23.7%, see Fig. 4b, a $L$ of ~ 5000 cd $m^{-2}$, $V_{ON} = 2.8$ V and a maximum $T_{50}$ of ~ 3 h, at $L = 150$ cd $m^{-2}$; $T_{50} = 15$ min, at $L = 1200$ cd $m^{-2}$ and $T_{50} = 3$ h, at $L = 150$ cd $m^{-2}$.

Gonzalez-Pedro *et al.* showed the positive passivation effect of the shelling of $CsPbX_3$ cores with amino-functionalized silanes on the PLQY.[72] On the other hand, Leng and coworkers[73] have reported the preparation of ultrathin core/shell structured $CsPbMnX_3$ PeNCs@$SiO_2$ composites (X = Cl, Br) through a reverse microemulsion method under room conditions. In this synthetic route, the addition of trioctylphosphine as a multibranched capping agent is pivotal to avoid the structural deterioration of the perovskite during the hydrolysis of silane species, also hindering the direct interaction between the nanocrystals and water molecules formed from the hydrolysis process. In this context, $Cs(Pb/Mn)X_3$ PENCSs@$SiO_2$ composites show an enhanced resistance to heat, with a PLQY of ~50.5%. Furthermore, this material does not exhibit any anion-exchange with other perovskite nanoparticles such as $CsPbBr_3$, maintaining its initial PL features. The mixture produced between the green- and stable yellow-light emissions from above Br- and Mn-PeNCs respectively can produce white-light emission without any signal of spectral shift, see Fig. 4c, combined with a blue on-chip LED device, generating white-LEDs (WLEDs) with an improved luminous efficiency of ~68.4 $lmW^{-1}$, correlated color temperature (CCT) ranging from 3857 K to 5934 K and a high color-rendering index (CRI) of ~90%, see Fig. 4d. This fact demonstrates the viability to fabricate white LEDs (WLEDs) with high color purity and suitable performance.

Table 1 Limitations and possible outcomes of perovskite/perovskite core/shell formation

| Limitations | Possible outcome |
|---|---|
| •The concept of epitaxy formation between iso- or multi-dimensional perovskites still needs to be disclosed properly, which is necessary to design wide varieties of perovskite core/shelling | • In the case of the 3D/2D system, the van der Waals epitaxy forms between the organic spacer of 2D perovskite with metal halide octahedra; therefore, the design of the organic molecule (spacer cation) with a suitable functional group for better interaction<br>• In the case of the 3D/3D and 3D/0D systems, it is important to understand the lattice constant of both the materials |
| •Two-step preparation method sometimes leads to the further abrupt growth of core materials alongside the growth of shelling materials | • Improved purification of the core materials is very important, since the unreacted precursors can react further to promote the control/abrupt growth<br>• Reaction parameters such as temperature and reaction time need to be considered for the growth of shelling materials |
| •Uncontrolled growth of the shelling material | • Dropwise addition of the shelling material as a function of time instead of one-time addition might help to prevent the uncontrolled growth of shelling materials<br>• Shelling must be done at considerably lower temperature to prevent a faster growth |

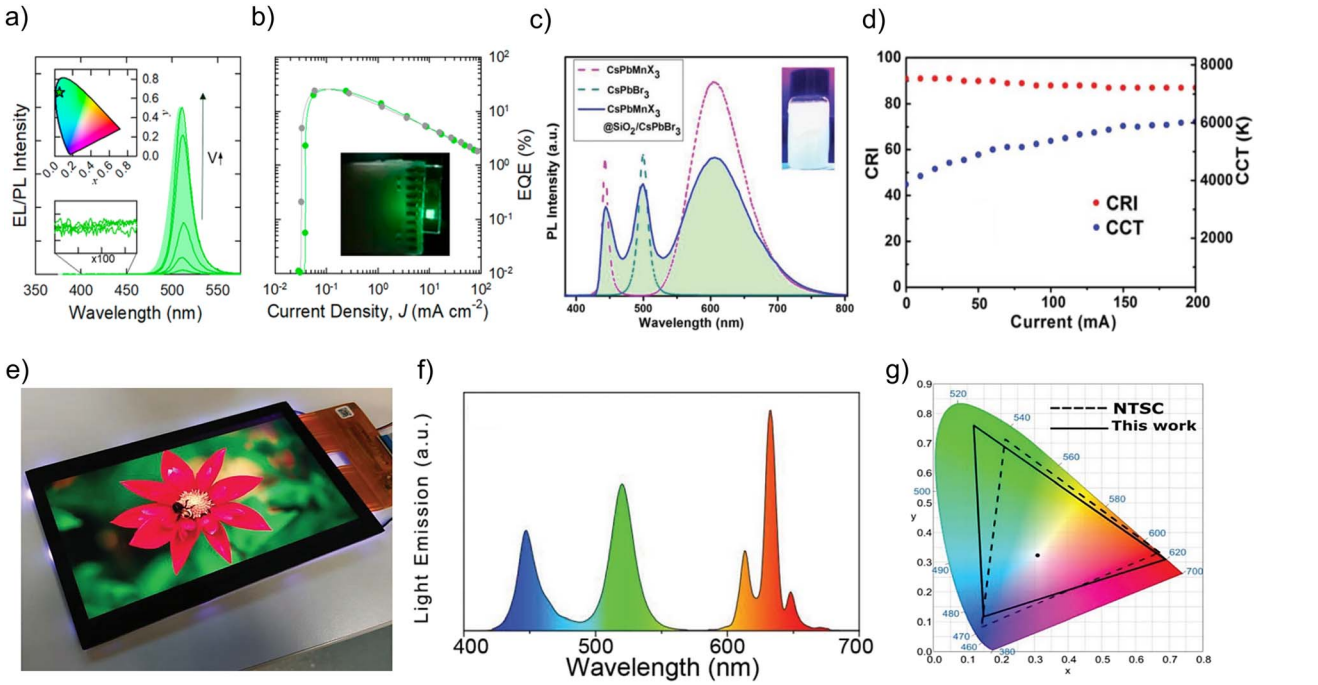


Fig. 4 (a) EL spectra and (b) EQE of ultrabright green-LEDs using PeNCs:$NiO_x$ composites as active layers. Reproduced under the terms of the CC-BY license.[71] Copyright 2023, The Authors. American Chemical Society. (c) Typical PL spectra of individual $CsPbBr_3$ (sea-green curve), $CsPbMnX_3$@$SiO_2$ (pink curve), and nanocrystal combination (blue curve) under UV illumination. The inset of Fig. 4c shows the white-light emission produced by the $CsPbBr_3$+ $CsPbMnX_3$@$SiO_2$ PeNC mixture. (d) CRI and CCT of a WLED device fabricated from the nanocrystal combination as a function of diverse driving currents during device operation. Reproduced with permission.[73] Copyright 2019, John Wiley & Sons, Inc. (e) Fabricated LCD display with its corresponding (f) PL spectrum and (g) estimated CIE color coordinates for white color emission produced by the LCD prototype (black line) compared with the NTSC standard color gamut area of CIE1931 (dashed line). Reproduced under the terms of the CC-BY license.[74] Copyright 2022, The Authors. John Wiley & Sons, Inc.

Dirin and coworkers[75] have developed the synthesis of colloidal $CsPbX_3$ PeNCs covered with metal oxide gel coatings by introducing non-hydrolytic sol–gel reactions. Here, alumina-, zirconia- and titania-based gel coatings were prepared and studied to improve the stability of PeNCs in polar environments. By reacting the corresponding metal halide $MX_3$ (M = Al, Zr, Ti; X = Cl, Br, and I) and metal alkoxide $M(OR)_3$ (R = *t*-Bu), the subsequent addition of the PeNC solution and the precipitation step with acetone, coated nanoparticles with a charged surface were obtained, being dispersible in water and some alcohols. At this stage, metal oxide gel coatings have replaced organic capping ligands from the material surface. While the crude gel-coated NCs contain excess gel, which can be washed away by precipitating them in a nonpolar to less-polar solvent (*e.g.*, diethyl ether or hexane), after several rounds of washing (up to 5), thin metal oxide gel coatings ~1 nm are achieved. However, some differences in the stability of the coatings influence the final PL properties of the PeNCs. The presence of an Al coating on PeNCs generates nanoparticles for any halide, with a full width and half maximum (FWHM) of ~20 nm and PLQY values up to 90%. In contrast, the Zr- and Ti-coatings are not efficient compared to their Al analogues, hindering the removal of part of Zr-coverage during the purification step (causing a decrease in PLQY to obtain values between 40 and 50%), or the complete quenching of the PL features in the presence of Ti-coverage. In this scenario, a titania layer can act as an electron scavenger, which in contrast could be beneficial for photocatalytic systems. Accordingly, some limitations emerge which hinder the synthesis of high-quality PeNC based composites such as the partial removal of the inorganic shell during the purification step, the reactivity of the shell itself or the use of precursors reactive towards the nanoparticle core, and those inorganic species that incorporate carrier traps into the perovskite, decreasing the optical performance in the final composite. Hence, the choice of a convenient metal oxide layer would be pivotal to establish which PeNC dispersions are suitable to enhance the optical performance of LED devices.

Interestingly, Manna and coworkers[76] have performed the synthesis of $CsPbBr_3$ PeNCs covered with a mesoporous $SiO_2$ layer (*m*-$SiO_2$), in the presence of stoichiometric contents of molten salts based on $NaNO_3$, $KNO_3$ and KBr salts, under room conditions, at 320–350 °C. Under these conditions, PeNCs@*m*-$SiO_2$ composites are obtained. These materials show a PLQY of ~89 ± 10%, stable PL performance up to 3 h at 180 °C, in saline water at 90 °C up to 24 h, even resisting into an aqua regia (strong acidic environment) system for at least 30 days. The main ions such as $K^+$ and $Br^-$ from the molten salts favor the compensation of surface defects in the nanocrystal. Accordingly, these materials were used as green-color converters into a prototype display, where the composite embedded into a polymer film was mounted into a customized 7-in. LCD system with a magenta LED backlight (composed of

a commercial blue-LED and a red-emitting $K_2SiF_6:Mn^{4+}$), see Fig. 4e. The final device produces a white-light emission, see Fig. 4f with CIE color coordinates of (0.3067, 0.3271), and a correlated color temperature of 6861 K, covering 92% of the NTSC standard color gamut area of CIE1931, see Fig. 4g. This color gamut is higher compared to that offered by a commercial phosphor LCD display, for instance, that contained in a Dell XPS 15 7590 laptop. This contribution highlights that high-quality PeNC composites can be used in real systems, focusing on future device commercialization.

### 2.4 Chalcogenide quantum dot/perovskite core/shell

From the other point of view, ligand exchange of PbS quantum dots (QDs) using perovskite precursors is a method used to epitaxially grow the perovskite matrix over the inorganic QDs by replacing the original organic ligands on the surface of the QDs with the perovskite precursors. PbS QD crystals have a rock salt structure that is compatible with perovskite, and this allows the perovskite to crystalize around the PbS QDs.[77] These systems offer the advantage of versatility, as different combinations of perovskite precursors and PbS size can be coordinated, thus tuning the final optical properties. For instance, a triple cation shell results in a favorable energetic alignment with the core of the dot, thus leading to improved solar cell performances.[78]

This strategy is also adopted in the case of PbS QD embedded perovskite matrices. Through a ligand exchange process, native oleates anchored to PbS QDs are replaced by a perovskite ligand (for instance, $FAPbI_3$ ligand), see Fig. 5a, and the polarity of the ligand itself makes them compatible with the polar solvent in which the perovskite is soluble. The perovskite matrix in the presence of the QDs will show different structural and optical properties.[79,80] It has been demonstrated that after annealing, a monolayer of the perovskite can be formed around the PbS QDs, and this guarantees passivation of the PbS structural defects, shielding them from degradation upon exposure to ambient air for a prolonged time, see Fig. 5b and b′, and enhancing their optical and electronic properties. Pb-halide passivation leads to PbS QDs/perovskite with optical properties that are well-described by a theoretical model, based on a type I finite-barrier heterostructure between the PbS QD and the perovskite matrix. Ning *et al.* have successfully synthesized polyheterocrystalline solid multiple core/shell $PbS/MAPbI_3$ NCs, characterized by an epitaxial junction. Due to the type I junction commented above, the quantum confined infrared emission coming from the PbS QD core fulfils the criteria for advanced LED device performances.[81] Finally, these PbS/perovskite systems are good candidates for short-wave infrared (SWIR) photodetectors. Yin *et al.*[82] fabricated photodiodes with an EQE enhancement of 2.5 times compared with control devices, reaching an internal quantum efficiency of over 90%. On the other hand, a large area application has been reported, in which the judicious choice of the solvent (specifically 2,6-difluoropyridine, DFP) led to the preparation of stable PbS QD colloidal solutions in the presence of the $MAPbI_3$ (MAPI) ligand (Fig. 5c). To provide a wide analysis of the photophysical properties of PbS QDs, nanoparticles were grown with a particle size, from 2.7 to 3.7 nm diameter, corresponding to excitonic absorption peaks from 855 to 1070 nm.[83] After the ligand exchange process, these absorption edges/PL peak positions were redshifted from 892 to 1127 nm, see Fig. 5d, associated with the reduction of the quantum confinement effect by the action of the perovskite ligand. This feature is pivotal to prepare IR absorption layers through blade-coating deposition and improve the performance of PbS QD-based solar cells achieving photoconversion efficiencies of ~8.7% (Fig. 5e).[83] Considering that an improved carrier mobility is favored into the IR-active layer, this feature could be pivotal to promote the carrier injection into the MAPI-capped PbS QDs and fabricate promising IR-LEDs with high optical performance.

An important aspect regarding the preparation of LEDs is that by tuning the distance between adjacent PbS quantum dots, it is possible to improve the LED efficiencies[84] to achieve the optimum balance between charge injection and radiative exciton recombination.[84] Moreover, by varying the size of the quantum dots, the emission wavelengths between 800 and 1850 nm can be tuned.

To summarize the positive effects of using core/shell PeNCs for fabricating efficient and stable LEDs, we can mention that the introduction of organic/inorganic shelling and the formation of different types of heterostructures promote the surface passivation of the perovskites. Mainly, the density of halide vacancies and non-coordinated Pb (and thereby the content of carrier traps) is suppressed, favoring the emergence of high-quality PeNC emitting layers with improved radiative recombination and high PLQY. In this context, the higher the PLQY, more efficient electrons-to-light conversion will be reached by the PeNC-based LEDs, enhancing their performance. Moreover, core/shell PeNCs can exhibit a longer PL lifetime compared to pristine PeNCs, and the composition of the core and shell materials can be modulated, so that their incorporation as emitting layers can produce multicolor LED devices with a brighter, more stable and consistent light emission during their operation. Simultaneously, the coverage of PeNCs with organic/inorganic shells avoids the direct interaction or permeation of oxygen or polar molecules such as water or alcohols, allows PeNC processing under harsh conditions such as acids, saline water, and high temperatures, and hinders the anion-exchange between different kinds of halide perovskites. These facts extend the long-term stability of luminescent materials. Therefore, the fabrication of efficient LEDs with EQE values close to 30%, with high luminance/current parameters, and the introduction of stable PeNCs as color converters into the real prototypes of LCD systems are possible, mediating the generation of white light emission with enhanced color quality and CRI. In this scenario and considering the above benefits of the core/shell PeNCs, the PeNC-based LEDs are considered as promising energy-efficient and rapidly developing lighting technologies for future commercialization.

## 3. Characterization

Shell-growth monitoring includes the morphology evolution and the real-time steady-state PL analysis. *In situ* measurement

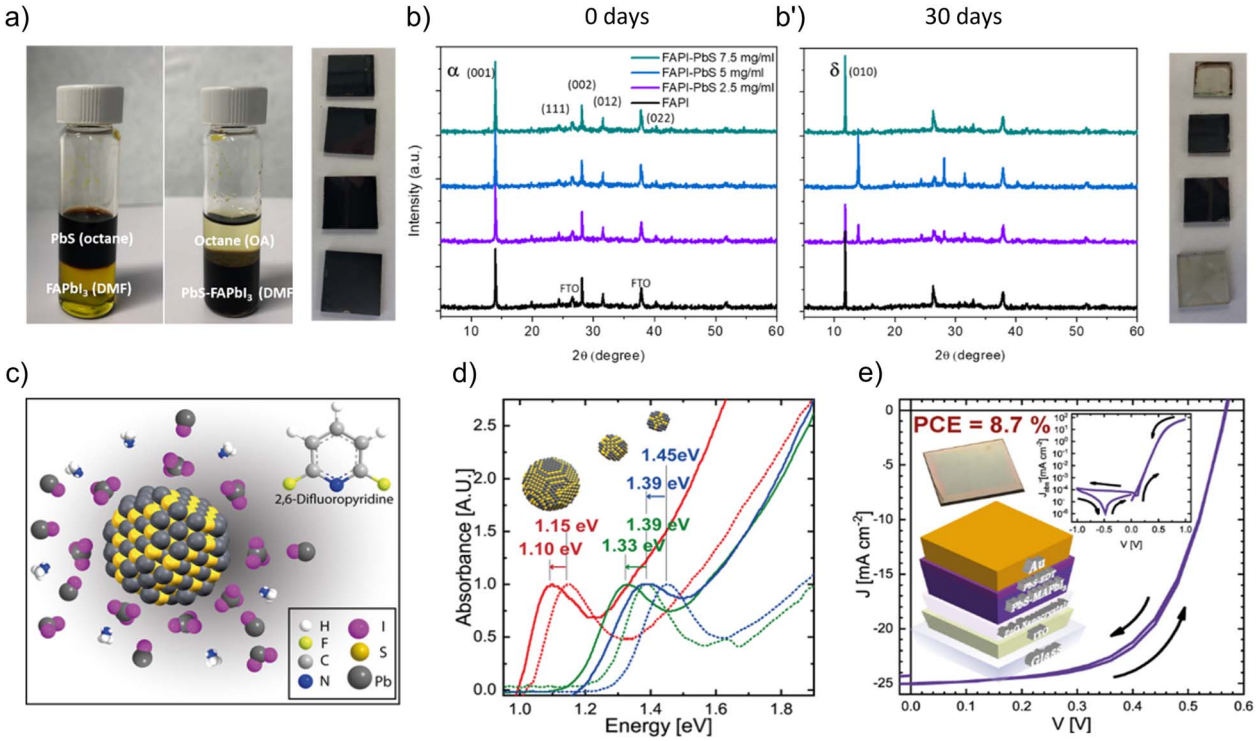


Fig. 5 (a) Photographs of the ligand exchange process between oleate-capped PbS QDs dispersed in octane and $FAPbI_3$ (FAPI) precursors: (i) before the interaction with $PbI_2$ + FAI in DMF and (ii) after the ligand exchange to produce FAPI-capped PbS QDs dispersed in DMF. (b) Typical XRD patterns of the FAPI films in the presence of different concentrations of PbS QDs at (b) 0 day and (b′) after 30 days of aging under ambient air. Reproduced from ref. 80 with permission, Copyright © 2020, American Chemical Society. (c) Schematic illustration of the stabilization of $MAPbI_3$-capped PbS QDs in the presence of DFP. (d) Optical properties of PbS QDs before (dashed lines) and after (solid lines) ligand exchange in the presence of DFP. (e) *J*–*V* characteristics of the record PbS QD based solar cell by using MAPI-capped PbS QD active layers. The inset of (e) exhibits the respective structure of the solar cell. Reproduced under the terms of the CC-BY-NC-ND license from ref. 83, Copyright © 2021, The Authors, American Chemical Society.

would allow time-resolved spectra to be recorded during the complete synthetic process, *i.e.*, during precursor mixing, warming-up, injection steps and so on. Therefore, PL and UV-vis would give complementary information: PL would be used to obtain spectrally resolved information about the nucleation kinetics, while UV-vis gives more information on the presence of intermediate phases during the material formation.[85] As an example, the fast nucleation and growth of $CsPbX_3$ nanocrystals following the hot-injection synthesis method have been investigated using the *in situ* steady state PL technique, where a broad and weak PL peak was detected at higher energy arising from the surfactant capping ligands and just after the third element injection (Cs-precursor or halide precursor), where a red-shifted narrow spectrum is observed.[1,86] In this context, the shelling mechanism can be investigated by detecting optical illusions occurring during the shelling process of the core-perovskite nanocrystals. A quantitative PL setup to measure PLQY and determine carrier lifetime would quantify radiative recombination over total recombination[42] to study the effects of shelling. In particular, organic shelling leads to minimizing the surface defects, as can be explained from this study. In addition, the PL lifetime of the core material after shelling is extended in comparison to the pristine core, as shown and explained in a previous section (Fig. 2a and c).[23,24] Simultaneously, UV-vis is one of the simplest and primary tools to study the absorbance evolution of shelling materials and can be carried out simultaneously with the *in situ* characterization of PL. *In situ* microscopy would prove invaluable in identifying the key features of heterojunctions in real time and would play a key role in the future design and implementation of such systems. Real-time TEM analysis enables the study of the evolution of the as-grown shelling material by studying the changes of shell thickness over time at different stages of reaction.[87] The TEM images of core/shell nanocrystals show a different contrast shelling over the core material (Fig. 1b and d), while the high-resolution TEM image shows epitaxial formation at the heterojunction of a core/shell (Fig. 2e). In terms of crystallite size changes, TEM analysis is the key tool to study successive particle size changes at different stages of shelling. This would enable the most relevant processes to be accurately monitored and understood and the optimal composition to be determined with high precision and reproducibility. Using the described high-resolution techniques, along with microscopy techniques, the morphology and electronic properties will be accessible. An understanding of the epitaxial matching between the core and the shell materials requires local or atomistic information.[87]

In perspective, the development of new characterization techniques based on Transmission Electron Microscopy (TEM)

also opened wide perspectives toward the understanding of the core–shell structure. Four-dimensional scanning TEM (4D-STEM) is an emerging technology to extract not only the intensity signal but also the phase information of the specimen.[88] Moreover, cation inversion at the interface in core–shell nanoparticles has been investigated recently by performing electron energy-loss spectroscopy (EELS) measurements with atomic resolution to map the ions in the shell and in the core structure.[89] In addition, by X-ray absorption spectroscopy (XAS) for determining the local geometric and/or electronic structure, the chemical composition and distribution of atoms in the crystal structure would be accurately determined.

In addition, the engineering of the LED device is straightforward and adheres to a traditional device architecture, which employs an inverted structure. In such a traditional configuration, a hole transport layer (PEDOT:PSS) is deposited, followed by a blocking layer (Poly-TPD), on top of an ITO-coated glass substrate. Next, the active layer consisting of core/shell perovskite NCs is deposited. On top of the active layer, an electron transport layer (PO-T2T or TPBi) is applied, followed by a buffer layer of LiF, and finally, aluminum is deposited.

## 4. Conclusion and prospects

Perovskite nanocrystals have recently been exploited for several optoelectronic applications. Common challenges in these systems such as thermodynamic stability and colour emission purity have been addressed. However, there is an unexplored area regarding tuning PeNC synthesis to reduce non-radiative recombination and core/shell structures can help enormously in this task. The knowledge of the free exciton and self-trap exciton phenomena along with control over the composition, growth and morphology of core/shell perovskite would broaden the prospects of real-world applications. The detailed understanding of the core/shell chemistry and mitigation of challenges aided by progress in synthesis and characterization will enable rapid advancement in this field. Inorganic and organic shelling orientation mechanisms and their impact on the stabilization of the perovskite core remain inadequately unexplored. In this regard, the optical properties of core/shell nanostructures, particularly colour emission stability, offer promising avenues for further improvement. Even though, for light management, highly emissive perovskite NCs already surpassed the conventional semiconductor quantum dots, *e.g.* chalcogenides, due to better colour tunability and narrow emission linewidth, the shelling strategies will improve the long-term stability,[90] focusing on their ultimate application in advanced technologies such as ultrahigh-definition commercial displays. Shelling of $CsPbBr_3$ NCs at the surface of inorganic microcrystalline carriers (NaBr) provides excellent stability against a vast variety of solvents, slightly narrowing the PL emission (~20 nm).[91] In this context, the future goal with such examples could be interesting for single crystal LED applications. Other interesting fields in which the core–shell strategy pays include the fabrication of large-area and flexible PeLEDs for display applications.[17] Moreover, the charge separation and carrier extraction at the heterojunction of type-II core/shell nanostructures can stimulate photocatalytic and photodetector applications.[24,36]

Furthermore, the core/shell system offers the possibility to change the fundamental properties of matter by changing the NC size and the shell thickness, thus making it strongly coupled to light.[92] Potentially, systems consisting of emitters separately surrounded by an inorganic shell look rather promising for polariton LEDs,[93] and in turn for developing high speed LEDs for communication systems. The potential of strong coupling to control light–matter interactions is far ranging with application in quantum information, polaritonic chemistry, lasing and even the development of novel coherent light sources.[94–96] Recent advances in heterostructures based on core/shell systems give ground to believe that the shell capping layer could indeed be used in many practical devices by exploiting the strong coupling effect.[97]

## Author contributions

S. D. A. was mainly responsible for writing the perspective. All co-authors were involved in writing a few parts of the perspective. All co-authors discussed the paper and revised the manuscript. S. M. was involved in providing the main idea and supervising the work.

## Conflicts of interest

The authors declare no conflict of interest.

## Acknowledgements

This work was supported by the Spanish Ministry of Science and Innovation under the Project Generación de Conocimiento SheLED (PID2021-122960OA-I00 supported by MCIN/AEI/10.13039/501100011033/and by FEDER Una manera de hacer Europa) and Project Transición Ecológica (TED2021-131600B–C3) STEP-UP, Generalitat Valenciana *via* Prometeo Grant Q-Solutions (CIPROM/2021/078). This work was supported by the European Innovation Council (EIC) *via* the OHPERA project (grant agreement 101071010). J. T. would like to acknowledge his Grant PRE2020-093444 funded by MCIN/AEI/10.13039/501100011033 and, as appropriate, by "ESF Investing in your future". S. M. acknowledges for the financial support from MICINN (Spain) through the program Juan de la Cierva-Incorporación IJC2020-042618-I.

## References

1 L. Protesescu, S. Yakunin, M. I. Bodnarchuk, F. Krieg, R. Caputo, C. H. Hendon, R. X. Yang, A. Walsh and M. V. Kovalenko, Nanocrystals of Cesium Lead Halide Perovskites (CsPbX3, X = Cl, Br, and I): Novel Optoelectronic Materials Showing Bright Emission with Wide Color Gamut, *Nano Lett.*, 2015, **15**, 3692–3696.

2 A. Dey, J. Ye, A. De, E. Debroye, S. K. Ha, E. Bladt, A. S. Kshirsagar, Z. Wang, J. Yin, Y. Wang, L. N. Quan, F. Yan, M. Gao, X. Li, J. Shamsi, T. Debnath, M. Cao,

M. A. Scheel, S. Kumar, J. A. Steele, M. Gerhard, L. Chouhan, K. Xu, X.-g. Wu, Y. Li, Y. Zhang, A. Dutta, C. Han, I. Vincon, A. L. Rogach, A. Nag, A. Samanta, B. A. Korgel, C.-J. Shih, D. R. Gamelin, D. H. Son, H. Zeng, H. Zhong, H. Sun, H. V. Demir, I. G. Scheblykin, I. Mora-Seró, J. K. Stolarczyk, J. Z. Zhang, J. Feldmann, J. Hofkens, J. M. Luther, J. Pérez-Prieto, L. Li, L. Manna, M. I. Bodnarchuk, M. V. Kovalenko, M. B. J. Roeffaers, N. Pradhan, O. F. Mohammed, O. M. Bakr, P. Yang, P. Müller-Buschbaum, P. V. Kamat, Q. Bao, Q. Zhang, R. Krahne, R. E. Galian, S. D. Stranks, S. Bals, V. Biju, W. A. Tisdale, Y. Yan, R. L. Z. Hoye and L. Polavarapu, State of the Art and Prospects for Halide Perovskite Nanocrystals, *ACS Nano*, 2021, **15**, 10775–10981.

3 J. Shamsi, A. S. Urban, M. Imran, L. De Trizio and L. Manna, Metal Halide Perovskite Nanocrystals: Synthesis, Post-Synthesis Modifications, and Their Optical Properties, *Chem. Rev.*, 2019, **119**, 3296–3348.

4 L. C. Schmidt, A. Pertegás, S. González-Carrero, O. Malinkiewicz, S. Agouram, G. Mínguez Espallargas, H. J. Bolink, R. E. Galian and J. Pérez-Prieto, Nontemplate Synthesis of CH3NH3PbBr3 Perovskite Nanoparticles, *J. Am. Chem. Soc.*, 2014, **136**, 850–853.

5 J. Luo, X. Wang, S. Li, J. Liu, Y. Guo, G. Niu, L. Yao, Y. Fu, L. Gao, Q. Dong, C. Zhao, M. Leng, F. Ma, W. Liang, L. Wang, S. Jin, J. Han, L. Zhang, J. Etheridge, J. Wang, Y. Yan, E. H. Sargent and J. Tang, Efficient and stable emission of warm-white light from lead-free halide double perovskites, *Nature*, 2018, **563**, 541–545.

6 J. Zhang, Y. Yang, H. Deng, U. Farooq, X. Yang, J. Khan, J. Tang and H. Song, High Quantum Yield Blue Emission from Lead-Free Inorganic Antimony Halide Perovskite Colloidal Quantum Dots, *ACS Nano*, 2017, **11**, 9294–9302.

7 M. Leng, Z. Chen, Y. Yang, Z. Li, K. Zeng, K. Li, G. Niu, Y. He, Q. Zhou and J. Tang, Lead-Free, Blue Emitting Bismuth Halide Perovskite Quantum Dots, *Angew. Chem., Int. Ed.*, 2016, **55**, 15012–15016.

8 F. Yan, S. T. Tan, X. Li and H. V. Demir, Light Generation in Lead Halide Perovskite Nanocrystals: LEDs, Color Converters, Lasers, and Other Applications, *Small*, 2019, **15**, 1902079.

9 F. Yan and H. V. Demir, LEDs using halide perovskite nanocrystal emitters, *Nanoscale*, 2019, **11**, 11402–11412.

10 J. Park, H. M. Jang, S. Kim, S. H. Jo and T.-W. Lee, Electroluminescence of Perovskite Nanocrystals with Ligand Engineering, *Trends Chem.*, 2020, **2**, 837–849.

11 A. Mohapatra, M. R. Kar and S. Bhaumik, Recent Progress and Prospects on Metal Halide Perovskite Nanocrystals as Color Converters in the Fabrication of White Light-Emitting Diodes, *Front. Electron. Mater.*, 2022, **2**, 891983.

12 A. Merdasa, M. Bag, Y. Tian, E. Källman, A. Dobrovolsky and I. G. Scheblykin, Super-Resolution Luminescence Microspectroscopy Reveals the Mechanism of Photoinduced Degradation in CH3NH3PbI3 Perovskite Nanocrystals, *J. Phys. Chem. C*, 2016, **120**, 10711–10719.

13 T. Wang, Z. Yang, L. Yang, X. Yu, L. Sun, J. Qiu, D. Zhou, W. Lu, S. F. Yu, Y. Lin and X. Xu, Atomic-Scale Insights into the Dynamics of Growth and Degradation of All-Inorganic Perovskite Nanocrystals, *J. Phys. Chem. Lett.*, 2020, **11**, 4618–4624.

14 J. Owen and L. Brus, Chemical Synthesis and Luminescence Applications of Colloidal Semiconductor Quantum Dots, *J. Am. Chem. Soc.*, 2017, **139**, 10939–10943.

15 R. Ghosh Chaudhuri and S. Paria, Core/Shell Nanoparticles: Classes, Properties, Synthesis Mechanisms, Characterization, and Applications, *Chem. Rev.*, 2012, **112**, 2373–2433.

16 M. R. Kar, S. Ray, B. K. Patra and S. Bhaumik, State of the art and prospects of metal halide perovskite core@shell nanocrystals and nanocomposites, *Mater. Today Chem.*, 2021, **20**, 100424.

17 G. H. Ahmed, J. Yin, O. M. Bakr and O. F. Mohammed, Successes and Challenges of Core/Shell Lead Halide Perovskite Nanocrystals, *ACS Energy Lett.*, 2021, **6**, 1340–1357.

18 S. Bera, B. Hudait, D. Mondal, S. Shyamal, P. Mahadevan and N. Pradhan, Transformation of Metal Halides to Facet-Modulated Lead Halide Perovskite Platelet Nanostructures on A-Site Cs-Sublattice Platform, *Nano Lett.*, 2022, **22**, 1633–1640.

19 J. Shi, W. Ge, J. Zhu, M. Saruyama and T. Teranishi, Core–Shell CsPbBr3@CdS Quantum Dots with Enhanced Stability and Photoluminescence Quantum Yields for Optoelectronic Devices, *ACS Appl. Nano Mater.*, 2020, **3**, 7563–7571.

20 W. Song, B. Zhang, W. Zhou, J. Zhang, L. Yu and S. Lian, Suppression of Thermal Quenching for CsPbX3 (X = Cl, Br, and I) Quantum Dots via the Hollow Structure of SrTiO3 and Light-Emitting Diode Applications, *Inorg. Chem.*, 2022, **61**, 19899–19906.

21 Y. Zeng, W. Chen, Y. Deng, W. Gu, C. Wu, Y. Guo, P. Huang, F. Liu and H. Li, FAPbBr3/Cs4PbBr6 Core/Shell Perovskite Nanocrystals with Enhanced Stability and Emission: Implications for LEDs, *ACS Appl. Nano Mater.*, 2022, **5**, 9534–9543.

22 F. Boussoufi, M. Pousthomis, A. Kuntzmann, M. D'Amico, G. Patriarche and B. Dubertret, Spray-Drying Polymer Encapsulation of CsPbBr3 Perovskite Nanocrystals with Enhanced Photostability for LED Downconverters, *ACS Appl. Nano Mater.*, 2021, **4**, 7502–7512.

23 V. K. Ravi, S. Saikia, S. Yadav, V. V. Nawale and A. Nag, CsPbBr3/ZnS Core/Shell Type Nanocrystals for Enhancing Luminescence Lifetime and Water Stability, *ACS Energy Lett.*, 2020, **5**, 1794–1796.

24 A. Kipkorir, J. DuBose, J. Cho and P. V. Kamat, CsPbBr3–CdS heterostructure: stabilizing perovskite nanocrystals for photocatalysis, *Chem. Sci.*, 2021, **12**, 14815–14825.

25 C. Ye, J. Jiang, S. Zou, W. Mi and Y. Xiao, Core–Shell Three-Dimensional Perovskite Nanocrystals with Chiral-Induced Spin Selectivity for Room-Temperature Spin Light-Emitting Diodes, *J. Am. Chem. Soc.*, 2022, **144**, 9707–9714.

26 C. Jia, H. Li, X. Meng and H. Li, CsPbX3/Cs4PbX6 core/shell perovskite nanocrystals, *Chem. Commun.*, 2018, **54**, 6300–6303.

27 X. Zhang, Z. Guo, R. Li, J. Yu, B. Yuan, B. Chen, T. He and R. Chen, Quasi-Type II Core–Shell Perovskite Nanocrystals for Improved Structural Stability and Optical Gain, *ACS Appl. Mater. Interfaces*, 2021, **13**, 58170–58178.

28 S. Wang, A. A. Yousefi Amin, L. Wu, M. Cao, Q. Zhang and T. Ameri, Perovskite Nanocrystals: Synthesis, Stability, and Optoelectronic Applications, *Small Struct.*, 2021, **2**, 2000124.

29 A. F. Gualdrón-Reyes, D. F. Macias-Pinilla, S. Masi, C. Echeverría-Arrondo, S. Agouram, V. Muñoz-Sanjosé, J. Rodríguez-Pereira, J. M. Macak and I. Mora-Seró, Engineering Sr-doping for enabling long-term stable FAPb1−xSrxI3 quantum dots with 100% photoluminescence quantum yield, *J. Mater. Chem. C*, 2021, **9**, 1555–1566.

30 F. Krieg, S. T. Ochsenbein, S. Yakunin, S. ten Brinck, P. Aellen, A. Süess, B. Clerc, D. Guggisberg, O. Nazarenko, Y. Shynkarenko, S. Kumar, C.-J. Shih, I. Infante and M. V. Kovalenko, Colloidal CsPbX3 (X = Cl, Br, I) Nanocrystals 2.0: Zwitterionic Capping Ligands for Improved Durability and Stability, *ACS Energy Lett.*, 2018, **3**, 641–646.

31 E. Hassanabadi, M. Latifi, A. F. Gualdrón-Reyes, S. Masi, S. J. Yoon, M. Poyatos, B. Julián-López and I. Mora-Seró, Ligand & band gap engineering: tailoring the protocol synthesis for achieving high-quality CsPbI3 quantum dots, *Nanoscale*, 2020, **12**, 14194–14203.

32 S. Bera and N. Pradhan, Perovskite Nanocrystal Heterostructures: Synthesis, Optical Properties, and Applications, *ACS Energy Lett.*, 2020, **5**, 2858–2872.

33 H. Wu, S. Wang, F. Cao, J. Zhou, Q. Wu, H. Wang, X. Li, L. Yin and X. Yang, Ultrastable Inorganic Perovskite Nanocrystals Coated with a Thick Long-Chain Polymer for Efficient White Light-Emitting Diodes, *Chem. Mater.*, 2019, **31**, 1936–1940.

34 V. A. Hintermayr, C. Lampe, M. Löw, J. Roemer, W. Vanderlinden, M. Gramlich, A. X. Böhm, C. Sattler, B. Nickel, T. Lohmüller and A. S. Urban, Polymer Nanoreactors Shield Perovskite Nanocrystals from Degradation, *Nano Lett.*, 2019, **19**, 4928–4933.

35 J. Zhang, P. Jiang, Y. Wang, X. Liu, J. Ma and G. Tu, In Situ Synthesis of Ultrastable CsPbBr3 Perovskite Nanocrystals Coated with Polyimide in a CSTR System, *ACS Appl. Mater. Interfaces*, 2020, **12**, 3080–3085.

36 C. Zhang, J. Chen, L. Kong, L. Wang, S. Wang, W. Chen, R. Mao, L. Turyanska, G. Jia and X. Yang, Core/Shell Metal Halide Perovskite Nanocrystals for Optoelectronic Applications, *Adv. Funct. Mater.*, 2021, **31**, 2100438.

37 V. Chiozzi and F. Rossi, Inorganic–organic core/shell nanoparticles: progress and applications, *Nanoscale Adv.*, 2020, **2**, 5090–5105.

38 M. G. Greiner, A. Singldinger, N. A. Henke, C. Lampe, U. Leo, M. Gramlich and A. S. Urban, Energy Transfer in Stability-Optimized Perovskite Nanocrystals, *Nano Lett.*, 2022, **22**, 6709–6715.

39 Y. Wang, L. Luo, Z. Wang, B. Tawiah, C. Liu, J. H. Xin, B. Fei and W.-Y. Wong, Growing Poly(norepinephrine) Layer over Individual Nanoparticles To Boost Hybrid Perovskite Photocatalysts, *ACS Appl. Mater. Interfaces*, 2020, **12**, 27578–27586.

40 J. S. Kim, J.-M. Heo, G.-S. Park, S.-J. Woo, C. Cho, H. J. Yun, D.-H. Kim, J. Park, S.-C. Lee, S.-H. Park, E. Yoon, N. C. Greenham and T.-W. Lee, Ultra-bright, efficient and stable perovskite light-emitting diodes, *Nature*, 2022, **611**, 688–694.

41 J. Song, O. Wang, H. Shen, Q. Lin, Z. Li, L. Wang, X. Zhang and L. S. Li, Over 30% External Quantum Efficiency Light-Emitting Diodes by Engineering Quantum Dot-Assisted Energy Level Match for Hole Transport Layer, *Adv. Funct. Mater.*, 2019, **29**, 1808377.

42 A. F. Gualdrón-Reyes, R. Fernández-Climent, S. Masi, C. A. Mesa, C. Echeverría-Arrondo, F. Aiello, F. Balzano, G. Uccello-Barretta, J. Rodríguez-Pereira, S. Giménez and I. Mora-Seró, Efficient Ligand Passivation Enables Ultrastable CsPbX3 Perovskite Nanocrystals in Fully Alcohol Environments, *Adv. Opt. Mater.*, 2023, 2203096.

43 P. Aggarwal, A. Halder, Neelakshi, R. Ramapanicker and V. Govind Rao, Energy Funneling from Water-Dispersed Perovskites to Chromophores, *ACS Energy Lett.*, 2023, **8**, 1520–1528.

44 S. R., V. Nayak, M. S. Jyothi and R. Geetha Balakrishna, Review on recent advances of core-shell structured lead halide perovskites quantum dots, *J. Alloys Compd.*, 2020, **834**, 155246.

45 H.-Y. Kim and Y.-S. Kim, P-123: Preparation of CsPbBr3/PbS Core/Shell Perovskite Quantum Dot for Enhanced Stability in Polar Solvent, *SID Symposium Digest of Technical Papers*, 2018, vol. 49, pp. 1670–1673.

46 X. Zhang, M. Lu, Y. Zhang, H. Wu, X. Shen, W. Zhang, W. Zheng, V. L. Colvin and W. W. Yu, PbS Capped CsPbI3 Nanocrystals for Efficient and Stable Light-Emitting Devices Using p–i–n Structures, *ACS Cent. Sci.*, 2018, **4**, 1352–1359.

47 E. Shi, Y. Gao, B. P. Finkenauer, Akriti, A. H. Coffey and L. Dou, Two-dimensional halide perovskite nanomaterials and heterostructures, *Chem. Soc. Rev.*, 2018, **47**, 6046–6072.

48 S. K. Dutta, S. Bera and N. Pradhan, Why Is Making Epitaxially Grown All Inorganic Perovskite–Chalcogenide Nanocrystal Heterostructures Challenging? Some Facts and Some Strategies, *Chem. Mater.*, 2021, **33**, 3868–3877.

49 J. Li, Z. Guo, S. Xiao, Y. Tu, T. He and W. Zhang, Optimizing optical properties of hybrid core/shell perovskite nanocrystals, *Inorg. Chem. Front.*, 2022, **9**, 2980–2986.

50 C. Zhang, S. Wang, X. Li, M. Yuan, L. Turyanska and X. Yang, Core/Shell Perovskite Nanocrystals: Synthesis of Highly Efficient and Environmentally Stable FAPbBr3/CsPbBr3 for LED Applications, *Adv. Funct. Mater.*, 2020, **30**, 1910582.

51 J. Xu, W. Huang, P. Li, D. R. Onken, C. Dun, Y. Guo, K. B. Ucer, C. Lu, H. Wang, S. M. Geyer, R. T. Williams and D. L. Carroll, Imbedded Nanocrystals of CsPbBr3 in Cs4PbBr6: Kinetics, Enhanced Oscillator Strength, and Application in Light-Emitting Diodes, *Adv. Mater.*, 2017, **29**, 1703703.

52 P. Cottingham and R. L. Brutchey, On the crystal structure of colloidally prepared CsPbBr3 quantum dots, *Chem. Commun.*, 2016, **52**, 5246–5249.

53 X. Tang, J. Yang, S. Li, W. Chen, Z. Hu and J. Qiu, CsPbBr3/CdS Core/Shell Structure Quantum Dots for Inverted Light-Emitting Diodes Application, *Front. Chem.*, 2019, **7**, 499.

54 X. Tang, J. Yang, S. Li, Z. Liu, Z. Hu, J. Hao, J. Du, Y. Leng, H. Qin, X. Lin, Y. Lin, Y. Tian, M. Zhou and Q. Xiong, Single Halide Perovskite/Semiconductor Core/Shell Quantum Dots with Ultrastability and Nonblinking Properties, *Adv. Sci.*, 2019, **6**, 1900412.

55 X. Liu, X. Zhang, L. Li, J. Xu, S. Yu, X. Gong, J. Zhang and H. Yin, Stable Luminescence of CsPbBr3/nCdS Core/Shell Perovskite Quantum Dots with Al Self-Passivation Layer Modification, *ACS Appl. Mater. Interfaces*, 2019, **11**, 40923–40931.

56 L. Wang, I. King, P. Chen, M. Bates and R. R. Lunt, Epitaxial and quasiepitaxial growth of halide perovskites: New routes to high end optoelectronics, *APL Mater.*, 2020, **8**, 100904.

57 S. S. Bhosale, S. Narra, E. Jokar, A. Manikandan, Y.-L. Chueh and E. W.-G. Diau, Functionalized hybrid perovskite nanocrystals with organic ligands showing a stable 3D/2D core/shell structure for display and laser applications, *J. Mater. Chem. C*, 2021, **9**, 17341–17348.

58 J. Fu, J. Liu, L. Yuan, Q. Pan, S. Chen, Y. Hu, J. Chen, W. Ma, Q. Zhang, Z. Liu and M. Cao, 3D/2D Core/Shell Perovskite Nanocrystals for High-Performance Solar Cells, *Small*, 2023, 2207312.

59 Y.-H. Kim, S. Kim, A. Kakekhani, J. Park, J. Park, Y.-H. Lee, H. Xu, S. Nagane, R. B. Wexler, D.-H. Kim, S. H. Jo, L. Martínez-Sarti, P. Tan, A. Sadhanala, G.-S. Park, Y.-W. Kim, B. Hu, H. J. Bolink, S. Yoo, R. H. Friend, A. M. Rappe and T.-W. Lee, Comprehensive defect suppression in perovskite nanocrystals for high-efficiency light-emitting diodes, *Nat. Photonics*, 2021, **15**, 148–155.

60 P. Serafini, A. F. Gualdrón-Reyes, R. S. Sánchez, E. M. Barea, S. Masi and I. Mora-Seró, Balanced change in crystal unit cell volume and strain leads to stable halide perovskite with high guanidinium content, *RSC Adv.*, 2022, **12**, 32630–32639.

61 P. Serafini, A. Villanueva-Antolí, S. Das Adhikari, S. Masi, R. S. Sánchez, J. Rodriguez-Pereira, B. Pradhan, J. Hofkens, A. F. Gualdrón-Reyes and I. Mora-Seró, Increasing the Performance and Stability of Red-Light-Emitting Diodes Using Guanidinium Mixed-Cation Perovskite Nanocrystals, *Chem. Mater.*, 2023, **35**(10), 3998–4006.

62 W. Chen, S. Bhaumik, S. A. Veldhuis, G. Xing, Q. Xu, M. Grätzel, S. Mhaisalkar, N. Mathews and T. C. Sum, Giant five-photon absorption from multidimensional core-shell halide perovskite colloidal nanocrystals, *Nat. Commun.*, 2017, **8**, 15198.

63 S. Huang, Z. Li, B. Wang, N. Zhu, C. Zhang, L. Kong, Q. Zhang, A. Shan and L. Li, Morphology Evolution and Degradation of CsPbBr3 Nanocrystals under Blue Light-Emitting Diode Illumination, *ACS Appl. Mater. Interfaces*, 2017, **9**, 7249–7258.

64 A. Loiudice, M. Strach, S. Saris, D. Chernyshov and R. Buonsanti, Universal Oxide Shell Growth Enables in Situ Structural Studies of Perovskite Nanocrystals during the Anion Exchange Reaction, *J. Am. Chem. Soc.*, 2019, **141**, 8254–8263.

65 Q. Zhong, M. Cao, H. Hu, D. Yang, M. Chen, P. Li, L. Wu and Q. Zhang, One-Pot Synthesis of Highly Stable CsPbBr3@SiO2 Core–Shell Nanoparticles, *ACS Nano*, 2018, **12**, 8579–8587.

66 Q. Zhong, J. Liu, S. Chen, P. Li, J. Chen, W. Guan, Y. Qiu, Y. Xu, M. Cao and Q. Zhang, Highly Stable CsPbX3/PbSO4 Core/Shell Nanocrystals Synthesized by a Simple Post-Treatment Strategy, *Adv. Opt. Mater.*, 2021, **9**, 2001763.

67 X.-C. Ru, J.-N. Yang, J. Ge, L.-Z. Feng, J.-J. Wang, K.-H. Song, T. Chen, Z. Yu Ma, L.-Y. Li and H.-B. Yao, Robust Sulfate Anion Passivation for Efficient and Spectrally Stable Pure-Red CsPbI3−xBrx Nanocrystal Light-Emitting Diodes, *Adv. Opt. Mater.*, 2023, 2300606.

68 Q. Zhong, X. Wang, M. Chu, Y. Qiu, D. Yang, T.-K. Sham, J. Chen, L. Wang, M. Cao and Q. Zhang, Ultra-Stable CsPbX3@Pyrophosphate Nanoparticles in Water over One Year, *Small*, 2022, **18**, 2107548.

69 X.-C. Ru, J.-S. Yao, J.-N. Yang, J. Ge, Y.-F. Lan, T. Chen, Z.-Y. Ma, Y.-C. Yin, J.-J. Wang, Y.-H. Song, L.-Z. Feng, K.-H. Song and H.-B. Yao, Microemulsion-Induced Stable CsPbBr3/PbWO4 Nanocrystals for Light-Emitting Diodes, *Adv. Photonics Res.*, 2022, **3**, 2100250.

70 J.-N. Yang, Y. Song, J.-S. Yao, K.-H. Wang, J.-J. Wang, B.-S. Zhu, M.-M. Yao, S. U. Rahman, Y.-F. Lan, F.-J. Fan and H.-B. Yao, Potassium Bromide Surface Passivation on CsPbI3-xBrx Nanocrystals for Efficient and Stable Pure Red Perovskite Light-Emitting Diodes, *J. Am. Chem. Soc.*, 2020, **142**, 2956–2967.

71 Q. Wan, W. Zheng, C. Zou, F. Carulli, C. Zhang, H. Song, M. Liu, Q. Zhang, L. Y. Lin, L. Kong, L. Li and S. Brovelli, Ultrathin Light-Emitting Diodes with External Efficiency over 26% Based on Resurfaced Perovskite Nanocrystals, *ACS Energy Lett.*, 2023, **8**, 927–934.

72 V. González-Pedro, S. A. Veldhuis, R. Begum, M. J. Bañuls, A. Bruno, N. Mathews, S. Mhaisalkar and Á. Maquieira, Recovery of Shallow Charge-Trapping Defects in CsPbX3 Nanocrystals through Specific Binding and Encapsulation with Amino-Functionalized Silanes, *ACS Energy Lett.*, 2018, **3**, 1409–1414.

73 X. Tang, W. Chen, Z. Liu, J. Du, Z. Yao, Y. Huang, C. Chen, Z. Yang, T. Shi, W. Hu, Z. Zang, Y. Chen and Y. Leng, Ultrathin, Core–Shell Structured SiO2 Coated Mn2+-Doped Perovskite Quantum Dots for Bright White Light-Emitting Diodes, *Small*, 2019, **15**, 1900484.

74 Z. Liu, L. Sinatra, M. Lutfullin, Y. P. Ivanov, G. Divitini, L. De Trizio and L. Manna, One Hundred-Nanometer-Sized $CsPbBr_3$/m-$SiO_2$ Composites Prepared via Molten-Salts Synthesis are Optimal Green Phosphors for LCD Display Devices, *Adv. Energy Mater.*, 2022, **12**, 2201948.

75 D. Guggisberg, S. Yakunin, C. Neff, M. Aebli, D. Günther, M. V. Kovalenko and D. N. Dirin, Colloidal CsPbX3 Nanocrystals with Thin Metal Oxide Gel Coatings, *Chem. Mater.*, 2023, **35**(7), 2827–2834.

76 M. N. An, S. Park, R. Brescia, M. Lutfullin, L. Sinatra, O. M. Bakr, L. De Trizio and L. Manna, Low-Temperature Molten Salts Synthesis: CsPbBr3 Nanocrystals with High Photoluminescence Emission Buried in Mesoporous SiO2, *ACS Energy Lett.*, 2021, **6**, 900–907.

77 J. Burschka, N. Pellet, S.-J. Moon, R. Humphry-Baker, P. Gao, M. K. Nazeeruddin and M. Grätzel, Sequential deposition as a route to high-performance perovskite-sensitized solar cells, *Nature*, 2013, **499**, 316–319.

78 M. Albaladejo-Siguan, D. Becker-Koch, A. D. Taylor, Q. Sun, V. Lami, P. G. Oppenheimer, F. Paulus and Y. Vaynzof, Efficient and Stable PbS Quantum Dot Solar Cells by Triple-Cation Perovskite Passivation, *ACS Nano*, 2020, **14**, 384–393.

79 T. T. Ngo, S. Masi, P. F. Mendez, M. Kazes, D. Oron and I. M. Seró, PbS quantum dots as additives in methylammonium halide perovskite solar cells: the effect of quantum dot capping, *Nanoscale Adv.*, 2019, **1**, 4109–4118.

80 S. Masi, C. Echeverría-Arrondo, K. M. M. Salim, T. T. Ngo, P. F. Mendez, E. López-Fraguas, D. F. Macias-Pinilla, J. Planelles, J. I. Climente and I. Mora-Seró, Chemi-Structural Stabilization of Formamidinium Lead Iodide Perovskite by Using Embedded Quantum Dots, *ACS Energy Lett.*, 2020, **5**, 418–427.

81 Z. Ning, X. Gong, R. Comin, G. Walters, F. Fan, O. Voznyy, E. Yassitepe, A. Buin, S. Hoogland and E. H. Sargent, Quantum-dot-in-perovskite solids, *Nature*, 2015, **523**, 324–328.

82 S. Yin, C. H. Y. Ho, S. Ding, X. Fu, L. Zhu, J. Gullett, C. Dong and F. So, Enhanced Surface Passivation of Lead Sulfide Quantum Dots for Short-Wavelength Photodetectors, *Chem. Mater.*, 2022, **34**, 5433–5442.

83 N. Sukharevska, D. Bederak, V. M. Goossens, J. Momand, H. Duim, D. N. Dirin, M. V. Kovalenko, B. J. Kooi and M. A. Loi, Scalable PbS Quantum Dot Solar Cell Production by Blade Coating from Stable Inks, *ACS Appl. Mater. Interfaces*, 2021, **13**, 5195–5207.

84 L. Sun, J. J. Choi, D. Stachnik, A. C. Bartnik, B.-R. Hyun, G. G. Malliaras, T. Hanrath and F. W. Wise, Bright infrared quantum-dot light-emitting diodes through inter-dot spacing control, *Nat. Nanotechnol.*, 2012, **7**, 369–373.

85 F. Babbe and C. M. Sutter-Fella, Optical Absorption-Based In Situ Characterization of Halide Perovskites, *Adv. Energy Mater.*, 2020, **10**, 1903587.

86 M. Do, I. Kim, M. A. Kolaczkowski, J. Kang, G. A. Kamat, Z. Yuan, N. S. Barchi, L.-W. Wang, Y. Liu, M. J. Jurow and C. M. Sutter-Fella, Low-dimensional perovskite nanoplatelet synthesis using in situ photophysical monitoring to establish controlled growth, *Nanoscale*, 2019, **11**, 17262–17269.

87 L. Yu, B. M. Hudak, A. Ullah, M. P. Thomas, C. C. Porter, A. Thisera, R. H. Pham, M. De Alwis Goonatilleke and B. S. Guiton, Unveiling the Microscopic Origins of Phase Transformations: An in Situ TEM Perspective, *Chem. Mater.*, 2020, **32**, 639–650.

88 A. Scheid, Y. Wang, M. Jung, T. Heil, D. Moia, J. Maier and P. A. van Aken, Electron Ptychographic Phase Imaging of Beam-sensitive All-inorganic Halide Perovskites Using Four-dimensional Scanning Transmission Electron Microscopy, *Microsc. Microanal.*, 2023, **29**(3), 869–878.

89 P. Torruella, A. Ruiz-Caridad, M. Walls, A. G. Roca, A. López-Ortega, J. Blanco-Portals, L. López-Conesa, J. Nogués, F. Peiró and S. Estradé, Atomic-Scale Determination of Cation Inversion in Spinel-Based Oxide Nanoparticles, *Nano Lett.*, 2018, **18**, 5854–5861.

90 J. Wang, D. Huang, Y. Zhou, C. Liao, P. Guo, Z. Li, G. Zhou, X. Yu and J. Hu, Enhanced Long-Term Luminescent Stability through Near-Single-Dot Passivation and Encapsulation of Perovskite Quantum Dots for Printable Photonics, *Small Struct.*, 2023, 2200391.

91 D. N. Dirin, B. M. Benin, S. Yakunin, F. Krumeich, G. Raino, R. Frison and M. V. Kovalenko, Microcarrier-Assisted Inorganic Shelling of Lead Halide Perovskite Nanocrystals, *ACS Nano*, 2019, **13**, 11642–11652.

92 M. Leng, J. Wu, K. Dini, J. Liu, Z. Hu, J. Tang, T. C. H. Liew, H. Sun, R. Su and Q. Xiong, Optically Pumped Polaritons in Perovskite Light-Emitting Diodes, *ACS Photonics*, 2023, **10**(5), 1349–1355.

93 T. Wang, Z. Zang, Y. Gao, C. Lyu, P. Gu, Y. Yao, K. Peng, K. Watanabe, T. Taniguchi, X. Liu, Y. Gao, W. Bao and Y. Ye, Electrically Pumped Polarized Exciton-Polaritons in a Halide Perovskite Microcavity, *Nano Lett.*, 2022, **22**, 5175–5181.

94 K. M. McCall, C. C. Stoumpos, S. S. Kostina, M. G. Kanatzidis and B. W. Wessels, Strong Electron–Phonon Coupling and Self-Trapped Excitons in the Defect Halide Perovskites A3M2I9 (A = Cs, Rb; M = Bi, Sb), *Chem. Mater.*, 2017, **29**, 4129–4145.

95 F. Stete, P. Schoßau, M. Bargheer and W. Koopman, Size-Dependent Coupling of Hybrid Core–Shell Nanorods: Toward Single-Emitter Strong-Coupling, *J. Phys. Chem. C*, 2018, **122**, 17976–17982.

96 A. C. Dakshinamurthy and C. Sudakar, Sublattice Distortion Enabled Strong Interplay between Phonon Vibrations, Electron–Phonon Coupling, and Self-Trapped Excitonic Emissions in Cs2Ag1–xNaxBiCl6 Double Perovskites, *J. Phys. Chem. Lett.*, 2022, **13**, 433–439.

97 K. Sartori, G. Cotin, C. Bouillet, V. Halté, S. Bégin-Colin, F. Choueikani and B. P. Pichon, Strong interfacial coupling through exchange interactions in soft/hard core–shell nanoparticles as a function of cationic distribution, *Nanoscale*, 2019, **11**, 12946–12958.